Journal of Water Process Engineering 71 (2025) 107153

Contents lists available at ScienceDirect

Journal of Water Process Engineering

journal homepage: www.elsevier.com/locate/jwpe

Exploring the potential of sewage sludge ash for CO_2 sequestration and resource recovery

M. Massa [a], S. Calce [a], P. Pachaiappan [a], B. Valentim [b], C. Punta [c], A. D'Anna [d], M. Blazina [d], Elza Bontempi [a,*]

[a] INSTM and Chemistry for Technologies Laboratory, Department of Mechanical and Industrial Engineering, University of Brescia, via Branze 38, Brescia 25123, Italy
[b] Earth Science Institute – Porto pole, Department of Geosciences, Environment and Spatial Plannings, Faculty of Sciences, University of Porto, rua do Campo Alegre s/n, 4169 – 007 Porto, Portugal
[c] Department of Chemistry, Materials, and Chemical Engineering "G. Natta" and INSTM Local Unit, Politecnico di Milano, Piazza Leonardo da Vinci 32, 20133 Milan, Italy
[d] MM SpA, Depuratore Milano San Rocco, Loc. Ronchetto delle Rane, 20141 Milano, Italy

ARTICLE INFO

Editor: Mohammad Mahdi A. Shirazi

Keywords:
Carbonation
Mineralization
P-recovery
Circular economy

ABSTRACT

The incineration of sewage sludge generates ash (SSA), which shows an increasing interest due to its potential for phosphorus recovery. The most promising application of SSA is as a fertilizer. However, direct use in agriculture faces significant challenges due to low nutrient bioavailability. Moreover, SSA has the potential for CO_2 capture through carbonation owing to their calcium content, which eventually increases the potential for P extraction due to the pH lowering. This study explores an experimental carbonation process applied to SSA, marking the first application of this technique to such waste. The carbonation was conducted in a high-pressure reactor in a fluid phase (slurry) to promote mineralization and the formation of carbonates. The better results were obtained for the SSA sample containing the higher calcite amount (about 28 %) with the capability to sequestrate about 20 kg of CO_2 for 1 ton of dry matter. Moreover, the results indicated that carbonation did not significantly improve the phosphorus leaching potential of the SSA compared to the untreated samples when acid extraction was performed. However, a strict correlation between the amorphous content and the P leachability was found for the first time, with a 0.7 % extraction efficiency for the sample with 15.2 % amorphous and 52.1 % extraction efficiency for the sample with 42 % amorphous. The results are promising for further research on optimizing the carbonation processes and exploring additional treatments to improve SSA's agricultural viability and CO_2 capture.

1. Introduction

Sewage sludge incineration is extensively practiced in some European countries (e.g., Netherlands, Switzerland, Austria, and Germany) [1] to eliminate the organic compounds and produce heat. By this process, sewage sludge ash (SSA) is generated, which concentrates some heavy metals and above all phosphorus (P) in the range of 4 % to 12 %, a level comparable to the P content found in (low-grade; 2 % to 18 % P) phosphate rock [2].

Multiple crystalline phases coexist in SSA, and their composition is influenced by the crystallization temperature and time for the thermal treatments realized on the sewage sludge [3]. These crystalline phases include quartz (SiO_2), hematite (Fe_2O_3), Al_2O_3, $AlPO_4$, zeolite, hydroxysodalite, whitlockite [$Ca_2(PO_4)_3$], anorthite, amorphous or poorly crystalline hydroxyapatite ($Ca_5(PO_4)_3OH$), and various phosphate minerals such $FePO_4$, $MgPO_4$, and whitlockite ($Ca_9Mg(PO_4)_6(PO_3OH)$) [4–7], which is the main P-bearing mineral phase in SSA and is commonly overgrown with hematite [5]. Moreover, an in-depth characterization shows that this waste contains amorphous phases in a variable amount [8].

Most of the P in SSA is present in low-soluble phases, and acid leaching is needed to recover more soluble phosphate phases [9]. However, the thermochemical treatment of sewage sludge ash with sodium salt additives was found to convert the $Ca_3(PO_4)_2$ component of raw SSA into buchwaldite ($NaCaPO_4$), resulting in distinct mineral phases with higher bioavailability to plants [10–12].

* Corresponding author.
E-mail address: elza.bontempi@unibs.it (E. Bontempi).

https://doi.org/10.1016/j.jwpe.2025.107153
Received 3 January 2025; Received in revised form 30 January 2025; Accepted 31 January 2025
Available online 8 February 2025

In brief, the possibilities of P extraction from SSA are limited. Still, its recycling may be possible in building applications since its chemical composition is similar to that of cement [13]. As such, SSA was tested as a binder or substitute for fine aggregates [14], as a partial cement replacement, and as an additive, in the production of mortars since the existence of an amorphous phase in SSA can boost the pozzolanic reaction during the later phases of concrete hardening [14].

Utilizing CaO-rich SSA as a partial substitute for fine aggregate can enhance the density of concrete, thereby leading to increased strength [15].

However, in some works, it is reported that SSA seems to show reduced pozzolanic activity compared to coal fly ash and other traditional supplementary cementitious materials due to differences in composition [16].

Still, the discrepancies found in the literature about the SSA composition and possible applications may be due to the differences in the sewage sludge combustion conditions, such as temperature, residence time, type of fluidizing material used, etc. In particular, an increase of temperature at values higher than 800 °C, for a residence time in a range of a few minutes, determines a progressive decrease of some heavy metals such as Zn, Cd, and Pb, due to volatilization, while Ni and Cr exhibit just a slightly increased mobility [17]. When the increasing temperature effect was investigated for longer residence times (3 h), an increase in the ceramic content (aluminosilicates) was also observed, together with the reduction of soluble salts (Na^+, K^+ and Mg^{2+}) [18]. Moreover, it has been also reported that a pre-stabilization by adding lime results in SSA with different mineralogical compositions and significantly higher activity than SSA produced following standard protocol [14,19].

Alkaline waste carbon dioxide sequestration is a sustainable process that utilizes industrial byproducts rich in alkaline compounds, such as calcium oxide (CaO) and magnesium oxide (MgO), to capture and store CO_2 in the form of stable carbonates. The process involves a chemical reaction where CO_2 reacts with alkaline phases in the waste, such as CaO or MgO, in the presence of water, forming stable minerals like calcium carbonate or magnesium carbonate. This reaction effectively locks the CO_2 in a solid and permanent form [20]. The sequestration process can follow two primary pathways. In direct carbonation, CO_2 is directly exposed to the solid waste in a controlled environment, often with added water to facilitate the reaction. Alternatively, indirect carbonation involves treating the waste to extract reactive components, which are then reacted with CO_2 to form carbonates. The efficiency of these processes is influenced by various factors. The physical properties of the waste, including particle size and surface area, are highly important, as smaller particles and higher surface areas increase the exposure of reactive sites, enhancing the carbonation reaction. Porosity further contributes by allowing better diffusion of CO_2 into the material, thereby improving the overall reaction rate [21]. Moisture content is another key factor, as water facilitates the dissolution of CO_2 and the subsequent formation of carbonate ions that drive the reaction. Similarly, higher CO_2 concentrations and pressures accelerate the process by increasing the solubility of CO_2 in the aqueous phase. Reaction time also influences the extent of carbonation, with longer durations generally leading to higher levels of carbonate formation. Temperature, meanwhile, must be carefully controlled, as moderate temperatures are optimal for carbonation; excessively high temperatures can reduce CO_2 solubility and favor competing reactions. Pre-treatment methods, such as grinding or thermal activation, can enhance the reactivity of alkaline wastes by exposing more reactive phases, thereby improving their carbonation potential. However, the presence of impurities or heavy metals may impact reaction kinetics and the stability of the resulting carbonates.

The carbonation process for several material typologies has been widely studied [22] and, over the past decade, there has been a significant advancement in the development of CO_2 mineralization and utilization of alkaline solid wastes [21,23], for example using carbonated rocks in deep geologic formations [22]. However, to the best of the authors' knowledge, no papers are reporting the capability of SSA to sequestrate CO_2.

Herein, a new possible application for SSA, sourced from an industrial facility in Northern Italy, is proposed for the first time to explore their CO_2 sequestration potential and to propose their application as secondary resources available at or near CO_2 emission sites [24]. This approach aligns with the actual need for limiting climate change by reducing the CO_2 in the atmosphere through mineralization. The impact of carbonation is also evaluated for its potential influence on phosphorus extraction efficiency.

2. Experimental

2.1. Materials

Three SSA samples were produced at a wastewater facility near Milan (Italy) featuring a waste-to-energy plant used to burn municipal sewage sludge (SS). SS is burned at 850 °C in a fluidized bed combustion chamber working with silica sand as bedding material, with an estimated residence time of 2–3 min. $CaCO_3$ is also added to control the acid gas emissions. Fig. S1 (Supplementary Materials) shows the process of water purification and sludge treatment before the incineration. Phosphorus removal from the wastewater is accomplished through a combination of chemical and biological processes. The biological process utilizes phosphorus-accumulating organisms (PAOs), while the chemical process involves the addition of ferric chloride ($FeCl_3$), which facilitates phosphorus precipitation. The precipitated phosphorus, in the $FePO_4$ form, is then effectively removed through filtration. Sample SS1 and SS2 are produced using a high dosage of $FeCl_3$ and low biological removal, while SS3 is produced using a low dosage of $FeCl_3$ and a higher biological removal. The dosage of $FeCl_3$ takes also part in the resulting color of the ashes: SSA_1 and SSA_2 have a darker red/brown color, while SSA_3 is lighter thanks to the higher dosage of PAOs for P removal and $CaCO_3$ for gas treatment. Specifically, the SS underwent a thickening process, to reduce the water content and volume of the sludge, and an aerobic stabilization to reduce the amount of organic matter and proliferation of pathogenic microorganisms (reducing the putrescibility) to improve the sludge management and disposal. Following these processes, the stage of dewatering, at a temperature of 100 °C, and/or thermal drying at a temperature of 270 °C take place.

Dewatered sludge is black, with a pungent odor and a shovelable muddy consistency (SS1 and SS3), containing 21–25 % of dry matter (DM). Thermally dried sludge also appears black, but it has an acrid, sharp odor and a dry, powdery texture containing 89–90 % of DM. The combined dried and dewatered sludge (mix) displays physical properties that balance the characteristics of both previous materials, containing 32–33 % of DM. The combustion of a mix of dewatered and thermally dried sludge allows to reduce the request of methane to support the combustion, i.e. about 45,5 Sm^3/ton.

The 3 SSA samples are obtained based on the following conditions:

- SSA_1: from SS1;
- SSA_2: from SS2;
- SSA_3: from SS1, after a bed material replacement (to improve the temperature control), a higher dosage of $CaCO_3$ (to control the acid gasses emissions), and a major P biological removal.

The calcium carbonate dosage to obtain SSA_3 was about 70–80 kg/ton of DM fed. Considering a dry matter content of 21–22 % in the sludge, the dosage corresponded to approximately 16 kg/ton of SS fed.

Fig. 1 shows the pictures of different materials treated and obtained at the incinerator plant (two SS typologies and three resulting SSA). The combustion of sewage sludge was carried out in the plant shown in Fig. S2 (Supplementary Materials) at 850 °C for 2 s according to the legislation [25]. The temperature is measured in the proximity of the internal combustion oven wall (Fig. S2). The reached temperature grants

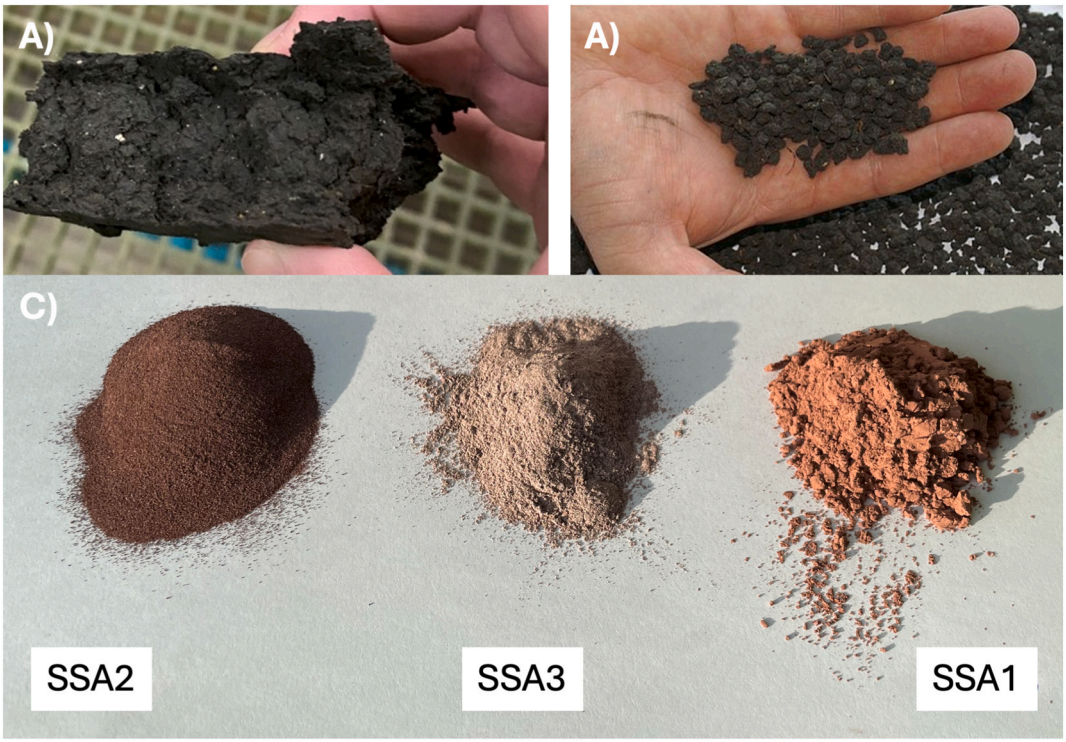

Fig. 1. Picture of dewatered (A) and thermal-dried (B) sewage sludge, resulting in a different amount of dry matter. Picture of the three resulting SSA (C) is also reported.

to converts the sludge into an inert material, the SSA. Dehydrated and/or dried sewage sludge is stored in two independent silos in the experimental area and fed separately into the furnace. From the hopper, dehydrated sludge is pumped into the furnace. Calcium carbonate is stored in a dedicated hopper and pneumatically dosed into the furnace. Dried sludge is pneumatically transferred to an injection lance in the therm-oxidative reactor, where thermal oxidation reactions occur. Gas flows are directed to the energy recovery section. The heat from the fumes is first transferred to cold air (via a heat exchanger) to ensure auto-combustion conditions, then to an air-water cooling circuit. Hot water is sent to a cooling tower for heat dissipation and recirculation. From energy recovery, fumes pass to the treatment unit, featuring dry (bag filters) and wet (scrubber) processes to meet emission limits. Purified fumes are released through the chimney, where continuous monitoring ensures compliance with regulations. Ashes from combustion and fume treatment systems are discharged into big bags in the ash unloading area. The SSA amount corresponds generally to about 10 % of the incinerated sewage sludge.

Ash characterization was conducted by ICP-OES to quantify total phosphorus and by X-ray diffraction with an internal standard to identify and quantify crystalline phases together with the amorphous content. Finally, SEM-EDS images were acquired to verify the condition of calcite crystals.

2.2. Acid digestion and wet extraction

The acid digestion was performed on 1 g of the SSA samples using 100 mL of aqua regia (HNO_3: HCl = 1:3, *v*/v) at 70 °C for 5 h to completely dissolve the powder and determine total P concentrations. The wet extraction was made according to the procedure described by Boniardi et al. [9]. In brief, the samples were stirred at room temperature with a liquid-to-solid ratio equal to 20 (e.g. 1 g of ash with 20 mL of H_2SO_4 0.2 M) and stirred for 2 h. After, the supernatant was filtered with a 0.45 μm nylon filter. HNO_3 (CAS n. 7697-37-2) with a purity >65 % and H_2SO_4 (CAS n. 7664-93-9) with a purity from 95 % to 97 % were purchased from Carlo Erba, and HCl (CAS n. 7647-01-0) with a purity of 37 % from Sigma-Aldrich.

2.3. Carbonation tests

The carbonation tests were made using a Berghof Reactor Heating System (BR – 300) working at ambient temperature (25 °C). The sequestration was carried out on a slurry composed of 35 g of each SSA sample studied in 45 mL of Milli-Q water (L/S = 1.5) that was magnetically stirred at 30 rpm for 24 h, and then dried at 105 °C in an electrical oven.

Considering CO_2 as an ideal gas [26], the CO_2 amount sequestrated by the carbonation was evaluated as:

$$n = P_{drop}\, V/RT \quad (1)$$

where P_{drop} is the pressure drop, V is the volume of the chamber occupied with gas (0.4 L), T is the settled reactor temperature (≈298 K) and R is the gas constant (0.08314472 L·bar/K·mol).

As a reference, the same volume of pure water was considered to evaluate CO_2 pressure variation [26]. This allows to consider the CO_2 water adsorption contribution. Then, the contribution of the water was subtracted to evaluate the pressure drop due to the sample. The amount of CO_2 consumed by the carbonation process was calculated using the measured pressure value.

2.4. Characterization techniques

2.4.1. X-ray diffraction (XRD)

All samples were characterized through X-ray diffraction (XRD) using an X'Pert Pro diffractometer (PANalytical, Malvern, UK) equipped with an X'Celerator detector and Cu anode (CuKalpha 1.5406 Å) operating at 40 KV and 40 mA. The samples were prepared by up-loading technique and the data was collected between 10 and 75° 2 Theta range. The analysis was carried out using an internal standard of alumina (c.a. 10 wt% provided by Carlo Erba – CAS N. 1344-28-1) to

perform a quantitative phase analysis (QPA) via Rietveld Refinement using Profex 5.2.2, and crystalline structures retrieved from different crystal structures databases reported in the Supplementary Materials (Table S1).

2.4.2. Scanning Electron Microscopy and Energy Dispersive X-ray Spectroscopy (SEM-EDS)

A detailed image analysis of the same samples was performed at the Materials Centre of the University of Porto (CEMUP, Portugal) using Scanning Electron Microscopy with Energy Dispersive Spectroscopy (SEM-EDS) to identify the new carbonate crystal formation. The samples were fixed on a sample holder with carbon tape and sputtered with a thin carbon film to enhance conductivity. The SEM-EDS experiments used an FEI Quanta 400 FEG ESEM/EDAX Genesis X4M operating in high vacuum mode at 15 kV and an instrument-specific 4.5 beam spot size setting. The secondary electron mode (SE) was used for topography analysis, and the backscattered electron detection mode (BSE) was used for phase identification. Semi-quantitative elemental analysis of selected zones was made by X-ray microanalysis (EDS).

2.4.3. Inductively Coupled Plasma Optical Emission Spectroscopy (ICP-OES) and pH

P content was determined by ICP-OES using a PerkinElmer Optima 8300 SD spectrometer, lines 213.617, 214.914 and 178.221, with a limit of detection (LOD) of 0.05 mg/L. Each measure was conducted in triplicate. Fluka 51474 TraceCERT was used as a reference standard (1002 mg/L ± 4 stock solution, further diluted according to what was required for each sample).

A pH-meter Metrohm, model 827 Lab (Origgio, Italy) was used to evaluate the pH of the solutions after leaching in Milli-Q water according to the procedure of the Italian Fertilizer Scientific Center: a liquid-to-solid ratio equal to 16.66 (3 g in 50 mL of Milli-Q water) with a mixing time of 30 min. The pH was also measured following leaching tests in H_2SO_4 0.2 M.

3. Results and discussion

3.1. Characterization of the as-received SSAs

ICP-OES chemical analysis revealed that the total amount of P is slightly different for the three analyzed samples: 7.79 ± 0.2 wt% (SSA_1), 8.27 ± 0.2 wt% (SSA_2) 6.19 ± 0.2 wt% (SSA_3), varying at most by about 2 wt%.

Table 2 lists the XRD results obtained for the SSA samples as received (XRD patterns are available in the Supplementary Materials (Figs. S3, S4 and S5). Crystalline phases containing phosphorous include whitlockite, which is the major P-bearing phase ranging between 7.5 and 11.1 wt%, hydroxyapatite, tetrapotassium pyrophosphate (only for SSA_1 and SSA_2), and monetite (only for sample SSA_3).

The other major crystalline phases composing the SSA samples studied (Table 2) include quartz from the silica sand used as bed material; calcite mainly in the SSA_3 sample due to the major dosage of carbonates to control the acid gasses emission; lime resulting from carbonates decomposition; portlandite resulting from lime hydration [27] naturally absorbing environmental moisture. This process can be resumed with the following reactions [27,28]:

$$CaCO_3 \rightarrow CaO + CO_2 \quad (2)$$

$$CaO + H_2O \rightarrow Ca(OH)_2 \quad (3)$$

This sequence of reactions explains why the $Ca(OH)_2$ content is the highest in the SSA_3 sample (12.6 wt%); high contents of hematite (Fe_2O_3), related to the chemical P removal using $FeCl_3$, and anhydrite ($CaSO_4$) were also detected in all SSA samples. The three samples underwent different combustion processes due to varying experimental conditions tested in the pilot furnace to identify the optimal operational parameters for SSAs production.

3.2. Forced carbonation results

Fig. 2 reports the results of carbonation tests made on SSA_2 regarding CO_2 pressure drop. Similar curves obtained from the other samples were added to Supplementary materials (Fig. S6).

SSA carbonation in an aqueous media is composed of different steps concerning the CO_2 dissolution from the gas to the solution, its migration to the liquid-solid interface, and the CO_2 diffusion through the solid passivation layer. Finally, at the active solid interface, the following chemical reaction of carbonation can occur [29,30]:

$$Ca(OH)_2 + CO_2 \rightarrow CaCO_3 + H_2O \quad (4)$$

$$2CaClOH + CO_2 \rightarrow CaCO_3 + H_2O + CaCl_2 \quad (5)$$

The process of generating calcium carbonate leads to the formation of a passivation layer, limiting the continued transportation of CO_2 to the reaction interface. Different reaction conditions can produce diverse deposition mechanisms of carbonation products influencing the passivation layer and the CO_2 diffusion over the reaction time.

The behaviour of the P curve (Fig. 2), as a function of the time, is linear in the initial stage of the reaction (till about 30–40 min). This is due to the step that controls the rate of CO_2 absorption, which is attributed to the diffusion of CO_2 through the liquid film close to the gas-liquid interface [29]. Then, the carbonation process proceeds with the migration of the dissolved carbon dioxide to the liquid-solid interface, followed by its diffusion in the passivation layer.

Finally, the reaction of calcium carbonate formation can occur at the solid interface [29].

Moreover, the controlling mechanism at the final stage was constituted by the CO_2 diffusion through the passivation layer. In this case, the carbonation chemical reaction was reported to be a first-order reaction, occurring only at the active interfaces of the ash. The reaction progress can be followed by checking the reactor temperature (Fig. 2). The increase in the reactor temperature is due to the exothermic nature of carbonation. Then the reaction appears to finish after about 14 h when the temperature reaches the baseline.

Table 1 shows the CO_2 absorbed values by the SSA samples, calculated according to the gas law, the Rietveld refinement and quantitative phase analysis (QPA). Data about QPA are reported in Table 2. Considering SSA_3 sample, about 20 kg of carbon dioxide is sequestrated by 1 ton of DM.

The observed results concerning CO_2 sequestration were influenced by the different pre-treatment methods of the SSA samples. The pre-treatment impacted the mineralogical and chemical composition of the SSA, particularly the content of calcium-based phases such as $CaCO_3$ and $Ca(OH)_2$, which are critical for carbonation reactions. In particular, SSA_3 showed the highest carbon dioxide sequestration efficiency, absorbing approximately 20 kg of CO_2 per ton of dry matter. This was attributed to its higher content of $CaCO_3$ and $Ca(OH)_2$, resulting from the specific pre-treatment involving a higher dosage of $CaCO_3$ during incineration. This enhanced its carbonation capacity compared to SSA_1 and SSA_2.

The CO_2 values from Rietveld refinement (Table 2) are always lower than those obtained by gas law, probably because only the crystalline calcite is quantified. This difference suggests the formation of amorphous calcite within the samples, especially for sample SSA_2, where this difference is more marked (approx. 0.4 g out of 30 g of material) between the two values. This scenario is supported by the SEM-EDS experiments (Fig. 3).

After carbonation, calcite crystals are found in various shapes and sizes (Fig. 3), probably due to the distinct experiment times of formation, reflecting a variance in the values of formation pressure. The resulting amount of sequestrated CO_2 ranges from 33.6 to 79.3 g/Kg SSA. This is mainly due to the amount of free Ca-phases in SSA, which

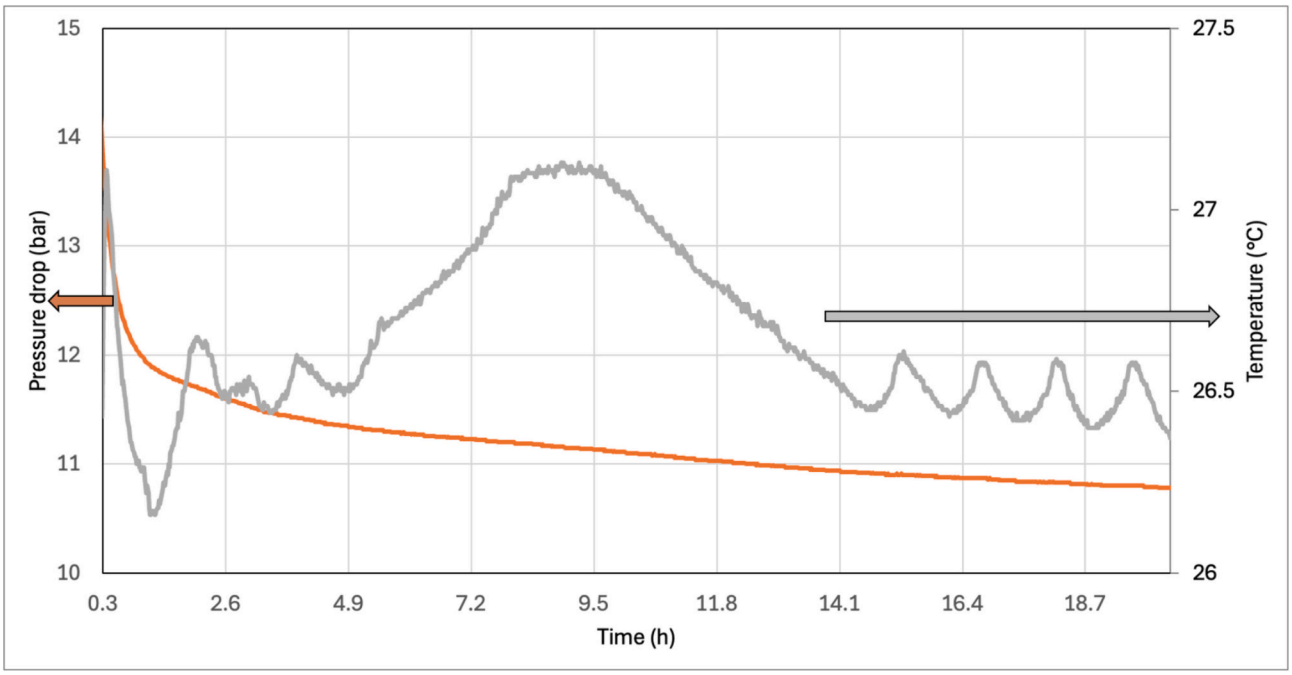

Fig. 2. Pressure drop and reactor temperature for SSA_2 sample during the carbonation experiment. The pressure drop shows a linear trend of data in the early stage of CO_2 diffusion. The temperature behaviour allows the highlight of the carbonation process.

Table 1
Evaluated pressure drop, and the corresponding amount of CO_2 sequestered by different SSA samples.

Sample	ΔP (bar)	ΔP (bar) drop (without P water drop)	CO_2 mass (g) absorbed by gas law	CO_2 mass (g) absorbed by QPA
SSA_1	4.74	1.84	1.16	0.91
SSA_2	4.50	1.60	1.01	0.60
SSA_3	6.68	3.78	2.38	2.27

are available to react with CO_2 forming $CaCO_3$ in stable form (calcite). The SSA_3 sample, the best performing of all SSA samples studied, also exemplifies this situation since it contains more Ca-phases (see Table 2).

3.3. X-ray data after CO_2 absorption

After the forced carbonation, the $CaCO_3$ content increased for all the samples (Table 2), reflecting the net CO_2 absorption capacity of 3.03 wt %, 2.02 wt%, and 7.56 wt% for SSA_1, SSA_2, and SSA_3, respectively.

However, the carbonation path was different in each one of the samples studied owing to their mineralogical composition as determined by XRD.

For SSA_1 the $CaCO_3$ content increases by about 6.9 wt% (Fig. S3) due to the complete carbonation of $Ca(OH)_2$ and calcium chloride hydroxide (CaClOH) crystalline phases according to the reactions (1) and (2) (Section 3.2) [30].

In this sample, however, a decrease in amorphous phase content was detected, probably due to the presence of Ca-amorphous phases that crystallized, forming calcite (see Table 2).

For SSA_2 and SSA_3 samples, after forced carbonation, an increase in calcite content of about 4.6 wt% and 17.2 wt%, respectively (Figs. S4 and S5), is related to the higher amounts of $Ca(OH)_2$ in the as-collected samples, highlighting that SSA_3 is the most suitable material to perform CO_2 capture. Other interesting reactions in SSA_3 involve crystalline phases with partial hydration of $CaSO_4$ into bassanite and gypsum and of monetite into brushite.

3.4. SEM-EDS analysis

SEM-EDS analysis was made on the as-collected and treated samples to highlight the formation of neoformation carbonates and the differences in the crystal shape and structure of the $CaCO_3$ particles.

As depicted in Fig. 3A, the topography of the particles in the as-collected samples revealed particles with a partially decomposed $CaCO_3$ structure, as evidenced by fragmentation, cracks and fissures, and loss of crystal angles and faces. This is caused by the thermal process and the stress the crystalline phases underwent during the combustion inside the waste-to-energy plant chamber.

However, on the samples submitted to forced carbonation, the crystallographic structure of some calcite seems partially restored (Fig. 3B), and one may see a covering of the surface of the particles by newly formed calcite crystals, which are nanometric (<40 nm) in SSA_2 sample (Fig. 3C) and not abundant since were not detected by XRD sample, and micrometric (1–4 μm) in size (Fig. 3D). A well-defined structure characterizes the latter; the planes of $CaCO_3$ accretion layering are well visible and typical of a deposition in a fluid system.

These differences in the newly formed $CaCO_3$ crystals are probably related to the trial's conditions, such as relative pressure set at 15 bar of CO_2 and decreasing during the 24-hour experiment.

During this period, accretion and deposition processes of $CaCO_3$ seemed to occur at the surface of the formerly decomposed crystals, thus allowing their restoration, evidenced by the development of a more defined structure, or acting as centers of nucleation for the newly formed crystals. For example, Fig. 3E and F show a partially decomposed $CaCO_3$ sand bed grain (approx. 80 μm) entirely covered with newly formed calcite nanocrystals.

These SEM-EDS results corroborate the XRD ones since $CaCO_3$ nanocrystals with a sub-crystalline structure are more typical of the SSA_2 sample than of SSA_1 and SSA_3. This validates the hypothesis of the presence of amorphous calcite in XRD results, where sample SSA_2 is the one with the greatest difference between CO_2 uptake values and between the results of the Rietveld refinement and recalculations from carbonation in the Berghof reactor according to the gas law.

Table 2
Quantitative phase analysis of SSAs before and after the carbonation trial and after the acid leaching. After carbonation, the samples are identified with "CO_2, and after leaching with "leached" (all the XRD patterns are reported in the Supplementary Materials).

Crystalline phases wt%		SSA_1	SSA_1 CO_2	SSA_2	SSA_2 CO_2	SSA_3	SSA_3 CO_2	SSA_1 leached	SSA_1 CO_2 leached	SSA_2 leached	SSA_2 CO_2 leached	SSA_3 leached	SSA_3 CO_2 leached
Anhydrite	$CaSO_4$	4.8	6.1	7.0	5.4	9.0	6.4	0.5	0.7	1	0.8	1.3	1.5
Bassanite	$CaSO_4{\cdot}0{,}5(H_2O)$						0.5						
Gypsum	$CaSO_4{\cdot}2H_2O$						0.4	46.5	47.9	47.8	48.1	63.95	59.5
Calcium hydroxychloride	CaClOH	0.9		0.4		0.5							
Lime	CaO	0.6		1.7		1.4							
Calcite	$CaCO_3$	7.7	14.6	10.6	15.2	28.2	45.4	0.7	0.5	0.7	2.2	3.6	6.2
Portlandite	$Ca(OH)_2$					12.6							
Goethite	FeO(OH)	1.3	0.6	1.1	1.2	0.5	0.6	0.4	0.4				0.5
Hematite	Fe_2O_3	9.7	8.3	9.3	7.9	4.4	3.9	11.1	10.3	10.1	9.6	3.9	3.9
Hydroxyapatite	$Ca_{10}(PO_4)_6(OH)_2$	3.6	3.3	5.4	3.6	4.7	3.0						
Tetrapotassium pyrophosphate	$K_4P_2O_7$	1.6	1.5	2.1	2.5								
Whitlockite	$Ca_9Mg(PO_4)_7$	11.0	10.6	11.1	9.8	7.5	6.5					4.5	2.5
Quartz	SiO_2	11.7	10.8	12.3	11.6	3.9	4.6	12.6	12.1	13.4	12.9	5.7	4.8
Sulfur	S_8	1.3	1.0	2.0	3.2	1.6	1.6						
Tridymite	SiO_2	2.1	2.2	1.5	2	3.8	1.2	2.3	2.6	4.3	5.1	1.9	3.6
Albite	$NaAlSi_3O_3$	0.9	2.3					2.7	2.2				
Magnesium sulfate	$MgSO_4$	0.2	0.4	0.9	0.7	1.0	0.4	0.5	0.6	0.8	1.1	0.5	0.4
Srebrodolskite	$Ca_2Fe_2O_5$	0.6	0.3	1.5	1.1	1.9	1.0	0.4	0.6	1.3	1.1	0.9	1
Monetite	$CaHPO_4$					3.1	2.9						
Magnesite	$MgCO_3$					0.7	0.5						
Brushite	$CaHPO_4{\cdot}2(H_2O)$						0.4						
Amorph		42.00	38.00	33.1	35.8	15.2	20.7	22.3	22.1	20.6	19.1	13.7	17.1
TOT		100.0	100.0	100.0	100.0	100.0	100.0	100.0	100.0	100.0	100.0	100.0	100.0
Crystalline phosphorous	P	3.21	3.04	3.65	3.11	3.05	2.6					0.92	0.51
Rwp		2.11	2.38	2.6	2.69	3.12	2.67	2.83	2.72	2.96	3.6	3.12	3.07

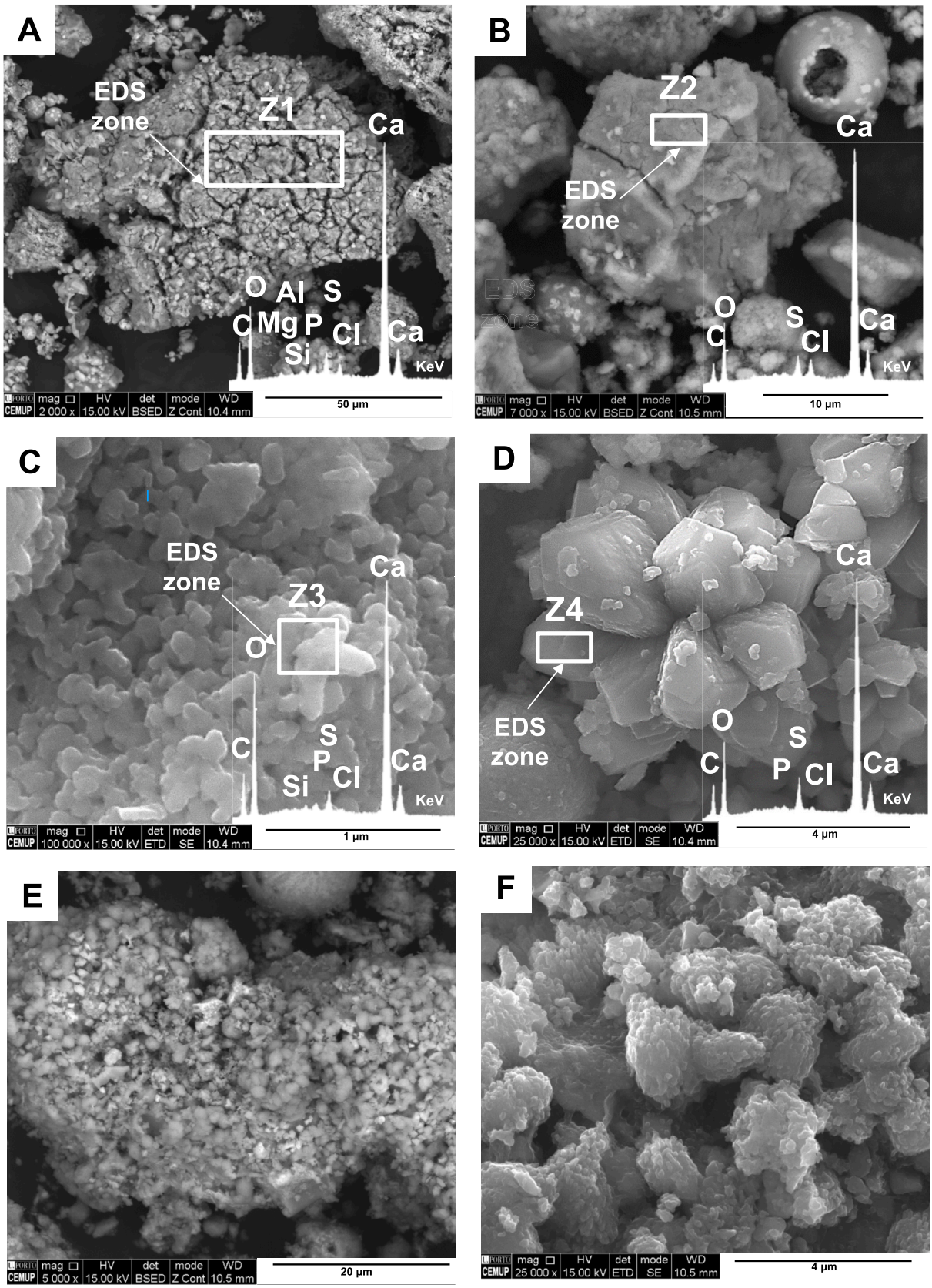

Fig. 3. SEM-EDS analysis of $CaCO_3$ before and after forced carbonation trials: A) partially decomposed $CaCO_3$ sand bed grain. EDS spectrum of zone Z1 (sample SSA_1; BSE mode; 2000×); B) restored calcite crystal. EDS spectrum of zone Z2 (sample of SSA_3; BSE mode; 7000×); C) newly formed calcite nanocrystals. EDS spectrum of zone Z3 (sample of SSA_2; SE mode; 100,000×); D) newly formed calcite crystals after forced carbonation (sample SSA_1; SE mode; 25,000×); E) surface of partially decomposed CaCO3 sand bed grain covered with newly formed calcite crystals (sample SSA_1; BSE mode; 5000×); F) magnification of "*E*" (sample SSA_1; SE mode; 25,000×).

3.5. Effect of SSA carbonation on P-extraction using H_2SO_4 0.2 M

As shown in Table 3, after carbonation, the pH of samples SSA_1 and SSA_2 decreases significantly from 12.6 to 7.5 and 7.7, respectively, while for SSA_3 decreases from 12.5 to 9.0. As stated in the literature [31] the extraction of P is generally found to be dependent on the final pH of the leaching solution, which is confirmed by the ICP-OES data in Table 3.

Thus, P-extraction tests were done with 0.2 M sulfuric acid and a 1:20 S/L ratio to see if a starting lower pH would increase P-extraction using the same amount of acid. Final pHs (Table 3) have some values for SSA_1 and SSA_1_CO_2, SSA_2 and SSA_2_CO_2 samples and the values of leached P (Table 3) are the same for the respective samples as-received and carbonated (e.g. SSA_1 P extraction = 40,606.4 ± 1000.7 mg/kg and SSA_1_CO_2 P extraction = 38,201.9 ± 1000.1 mg/kg). The values of P extraction for the carbonated samples were recalculated according to the CO_2 factor dilution.

The P extraction efficiency values are very similar: about 51–52 % for SSA_1 and SSA_1_CO_2 and 37–39 % for SSA_2 and SSA_2_CO_2 of the total P (Table 3). On the other hand, the leaching solutions pH of SSA_3 as-collected and SSA_3_CO_2 samples are different: 7.7 and 5.0, respectively. However, this difference is not significant for an increase in P-extraction since above a pH of 5.0 the P-extraction is low on these materials as shown in the literature [31].

This was not enough despite lowering the starting pH after carbonation since the acid needed to decrease the pH is almost the same, resulting in the impossibility of enhancing the P-extraction by carbonation.

The values of P-extraction (Table 3), remain unchanged for SSA_1 and SSA_2 samples. In sample SSA_3_CO_2, the absorbed CO_2, then released in the liquid phase during leaching, promotes a lower final pH value (5.0) such that a minimal P extraction (1829.5 ± 40.0 mg/kg) is boosted. Thus, the SSA_3 sample is the only one with a difference in P extraction due to the carbonation process. Still, the extraction values, no higher than 3.2 % of total P, do not justify this approach if aimed at improving extraction.

This can be attributed to the fact that carbonate addition in the incineration facility cannot promote the increase in P extraction efficiency. Calcium carbonate indeed can undergo a reaction with the acid extraction solution, resulting in the formation of carbon dioxide, water, and a corresponding salt, for example, calcium chloride or calcium oxalate, and gypsum [32]. Consequently, there is a reduced availability of acid (H^+) for the extraction of phosphorus, [33,34] which dissolves to a lesser extent [35].

The high $CaCO_3$ content of SSA_3 influences the phosphorus extraction, but not entirely in a positive way. Indeed, The SSA_3 sample, with its higher $CaCO_3$ content, showed a higher final pH of 5.0 after carbonation and acid leaching. It is known that low pH can facilitate phosphorus extraction; indeed, the observed P extraction efficiency was still minimal at 3.2 %, much lower than that of SSA_1 and SSA_2. This was justified by the presence of high amounts of $CaCO_3$ leading to reactions with the acid (H_2SO_4) during leaching, forming byproducts such as gypsum ($CaSO_4{\cdot}2H_2O$) and consuming available acid. This reaction reduces the free hydrogen ion concentration (H^+), limiting the dissolution of phosphorus-bearing phases like whitlockite. The SSA_3 sample also had a lower amorphous content compared to SSA_1 and SSA_2. Since phosphorus in SSA is more extractable from amorphous phases than crystalline phases, this appears to reduce the phosphorus extraction efficiency.

3.6. X-ray data after H_2SO_4 leaching on the solid residue

By Rietveld refinement, it was possible to quantify the amount of crystalline P bonded in the phosphate structures: 3.21 wt%, 3.65 wt%, and 3.05 wt%, for SSA_1, SSA_2, and SSA_3 respectively. These values indicated that some P is hosted in the amorphous phase, which results in 42.0 wt%, 33.0 wt%, and 15.2 wt% for samples SSA-1, SSA_2 and SSA_3, respectively, corresponding to a percentage of P ranging from 3.14 wt% (SSA_3) to 4.62 wt% (SSA_2). Fig. 4, reporting the P amount determined by chemical analysis in the SSA samples and the corresponding amount of amorphous P determined by Rietveld refinement, shows that P in the amorphous is higher than that corresponding in the crystalline phases, following the literature [5].

Table 2 lists the mineralogical results for solid residues obtained after acid leaching with 0.2 M of H_2SO_4. The carbonated and untreated samples (SSA_1_leach, SSA_2_leach and SSA_1_CO_2_leach, SSA_2_CO_2_leach), showed complete leaching of phosphorus-containing crystalline phases, since whitlockite, hydroxyapatite, and tetrapotassium pyrophosphate were not detected. For sample SSA_3, instead, it was found that the acid dosage was not enough to perform complete leaching of the crystalline phases since some whitlockite is still detected in the samples: approx. 4.5 wt% and 2.5 wt% for the as-collected and treated samples, respectively. However, other P-crystalline phases (e.g. monetite and hydroxyapatite) were not detected, and are assumed to be completely leached.

In addition, some components are not leachable and reflect pre-leaching values, for example, Fe_2O_3 and SiO_2.

The amorphous fraction of samples SSA_3 and SSA_3_CO_2 remains almost constant after the leaching test, decreasing by 2–3 wt%, while the amorphous fraction of samples SSA_1 and SSA_2 and respective carbonated products decrease by approximately 10–20 wt% after acid leaching. This difference indicates that part of the amorphous fraction is leachable at a low pH of about 1.6 (SSA_1 and SSA_2) while at a higher pH (SSA_3) the amorphous fraction remains almost unaltered.

The most abundant crystalline phase of the leached ashes is gypsum (Table 2), forming due to the interaction of sulfur (S) with Ca. This is because the system, after the usage of H_2SO_4 as a leaching agent, is highly enriched of S. Gypsum percentages are very high for treated and untreated samples: 46 wt%, 48 wt% and 60 wt%, for SSA_1 and SSA_2 and SSA_3, respectively.

The efficiency in P extraction (before and after carbonation – data in Table 3) appears to be influenced by the amorphous content of the samples. Fig. 5 shows that a strong correlation is established, suggesting a lower capability of the amorphous phase in trapping P, in comparison to the corresponding crystalline ones. Even if no data are available in the literature about this evidence for SSA, a reduction in the crystallinity of hydroxyapatite corresponds to an increase in its dissolution rate [36]. This confirms that the leaching is effective in extracting P available in the amorphous phase and strongly suggests that for these samples, the pH may not have the predominant role in the P leachability. This

Table 3
pH and P extraction for all samples and corresponding carbonated SSA (CO_2 refers to carbonated samples).

Sample	P tot mg/kg			pH	pH H_2SO_4 treated	P extraction mg/kg			Extraction efficiency %
SSA_1	77,873.2	±	1561.5	12.6	1.6	40,606.4	±	1000.7	52.1
SSA_1 CO_2	74,974.1	±	1503.4	7.5	1.6	38,201.9	±	1000.1	51.0
SSA_2	82,719.9	±	1559.6	12.6	1.6	30,910.7	±	999.7	37.4
SSA_2 CO_2	80,025.8	±	1508.8	7.7	1.6	31,189.1	±	999.7	39.0
SSA_3	61,892.1	±	1558.6	12.5	7.7	442.0	±	20.0	0.7
SSA_3 CO_2	57,449.8	±	1446.7	9.0	5.0	1829.5	±	40.0	3.2

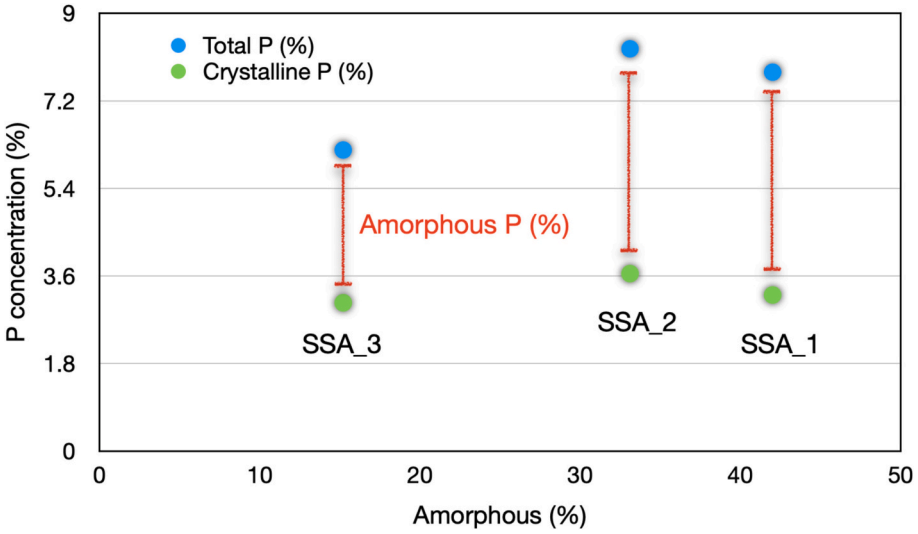

Fig. 4. Total P amount (%), determined by chemical analysis of digested sample. P in crystalline and amorphous phases (%) evaluated by Rietveld analysis is also reported.

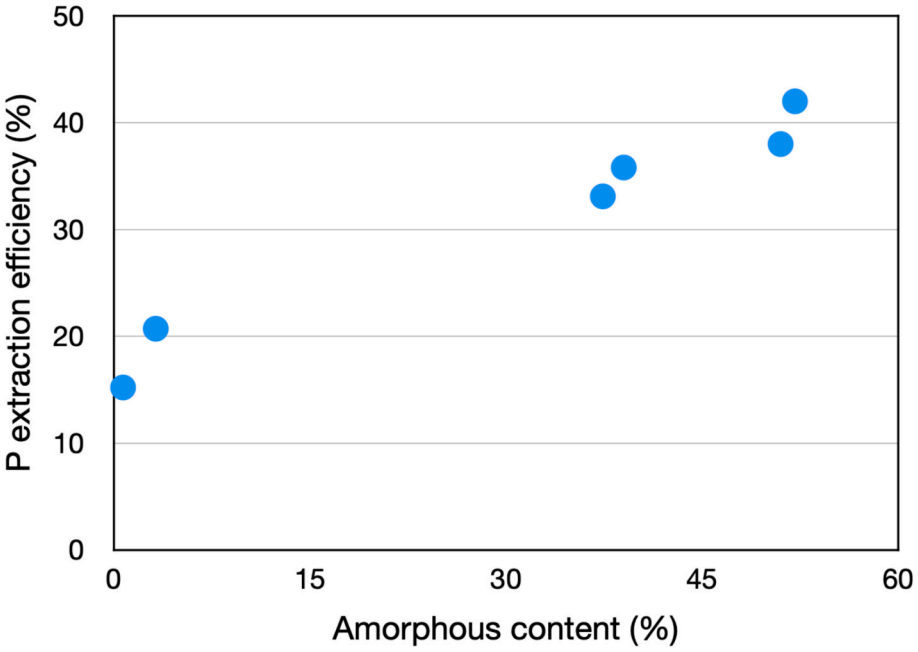

Fig. 5. P extraction efficiency (data reported in Table 3) versus the amount of amorphous phase.

strongly suggests that apart from an investigation of the most suitable oven temperature, by controlling the SSA cooling temperature after the SS incineration, it would be possible to increase the amorphous content in SSA, with the possibility to enhance the recovery efficiency and overall quality of the extracted phosphorous.

4. Feasibility

The results of this work allow us to discuss the feasibility of the proposed technology in terms of challenges and opportunities.

Among the challenges, the variability in SSA properties due to pre-treatment methods poses significant limitations, as it affects both CO_2 sequestration capacity and phosphorus recovery efficiency. Operational issues, such as scaling the carbonation process for industrial use and managing the environmental impacts of residuals, also require consideration. Additionally, the economic feasibility of employing SSA for CO_2 sequestration and resource recovery, including costs related to acid leaching and the handling of $CaCO_3$-rich samples, represents a critical hurdle.

Despite these challenges, this work offers significant opportunities. SSA demonstrates a dual potential for CO_2 sequestration and resource recovery, aligning with circular economy principles by converting waste into valuable resources. The integration of SSA-based processes near emission sources could enhance efficiency by reducing transportation needs. Moreover, tailored pre-treatment methods could optimize SSA's performance, opening pathways for future research and industrial applications.

This study also contributes meaningfully to several SDGs. It supports SDG 13 (Climate Action) by providing an innovative approach to mitigating CO_2 emissions. Promoting the reuse of industrial byproducts, minimizing waste, and recovering valuable resources, it aligns with SDG 12 (Responsible Consumption and Production). The phosphorus

recovery aspect directly supports SDG 2 (Zero Hunger), as the recovered phosphorus can be used to produce fertilizers essential for sustainable agriculture. Additionally, phosphorus recovery contributes to SDG 6 (Clean Water and Sanitation) and SDG 14 (Life Below Water) by addressing the issue of eutrophication in aquatic ecosystems, which is caused by excessive phosphorus runoff. This underscores the broader implications of the research, emphasizing its potential to address critical environmental challenges while advancing global sustainability efforts [37].

5. Conclusions

Sewage sludge ash samples were characterized using X-ray diffraction and ICP-OES to identify and quantify the minerals, quantify the amorphous phase, and determine the total P amount.

The P is mostly contained in the amorphous fraction of the samples but is also present in crystalline phases mainly in whitlockite, hydroxyapatite, tetra potassium pyrophosphate (in samples SSA_1 and SSA_2), and monetite (in sample SSA_3).

CO_2 forced carbonation trials were conducted on all samples causing mineralization on the SSA particles surface, which was confirmed with SEM-EDS: partially decomposed Ca-phases underwent a “restoration” process characterized by newly formed crystal faces and the growth of nano and micrometric $CaCO_3$ crystals.

However, the best forced carbonation results were obtained for sample SSA_3, which appears to capture about 20 kg of CO_2 for 1 ton of dry matter which is a promising result for using this type of SSA for CO_2 mineralization.

The carbonation of SSA enables the lowering of the pH of the ashes. Still, the amount of extracted P using H_2SO_4 0.2 M doesn't change and it is not enough to justify this method to improve phosphorus extraction via acid leaching. However, it is shown that the highest the amorphous content in SSA, the highest is P extraction efficiency.

This method offers several advantages, including the permanent storage of CO_2 in a stable and non-leachable form, the reuse of industrial waste in alignment with circular economy principles, and the potential application of carbonated products in industries such as construction, where they can serve as supplementary cementitious materials. However, the process optimization, by changing some of the influencing parameters, is not considered in this phase and would object to future research to maximize CO_2 uptake. Overall, SSA waste CO_2 sequestration could represent a promising solution for reducing emissions while repurposing industrial byproducts, contributing to both climate change mitigation and resource recovery.

CRediT authorship contribution statement

M. Massa: Writing – original draft, Formal analysis, Data curation, Conceptualization. **S. Calce:** Methodology, Investigation. **P. Pachaiappan:** Investigation. **B. Valentim:** Writing – review & editing, Funding acquisition, Formal analysis, Data curation. **C. Punta:** Validation, Methodology, Investigation, Formal analysis. **A. D'Anna:** Validation, Resources, Investigation, Formal analysis. **M. Blazina:** Investigation, Funding acquisition, Formal analysis. **Elza Bontempi:** Writing – review & editing, Writing – original draft, Resources, Project administration, Investigation, Funding acquisition, Formal analysis, Conceptualization.

Declaration of competing interest

The authors declare that they have no known competing financial interests or personal relationships that could have appeared to influence the work reported in this paper.

Acknowledgements

This work was supported by RHIGUS (LOW ENERGY TECHNOLOGIES FOR RECOVERY OF HIGH-GRADE PHOSPHORUS) financed by MUR: PRIN 2022.

This work was also supported under the scope of the Next-GenerationEU (Italian PNRR – M4 C2, Invest 1.3 – D.D. 1551.11-10-2022, PE00000004) within the MICS (Made in Italy–Circular and Sustainable) Extended Partnership.

B.V. thanks national funds through FCT - Fundaçao para a Ciencia e Tecnonologia, I.P., in the framework of the UIDB/04683 and UIDP/04683 Instituto de Ciencias de la Terra programs.

Appendix A. Supplementary data

Supplementary data to this article can be found online at https://doi.org/10.1016/j.jwpe.2025.107153.

Data availability

Data will be made available on request.

References

[1] H. Herzel, O. Krüger, L. Hermann, C. Adam, Sewage sludge ash - a promising secondary phosphorus source for fertilizer production, Sci. Total Environ. 542 (2016) 1136–1143, https://doi.org/10.1016/j.scitotenv.2015.08.059.
[2] S. Liang, L. Yang, H. Chen, W. Yu, S. Tao, S. Yuan, K. Xiao, J. Hu, H. Hou, B. Liu, J. Yang, Phosphorus recovery from incinerated sewage sludge ash (ISSA) and reutilization of residues for sludge pretreated by different conditioners, Resour. Conserv. Recycl. 169 (2021), https://doi.org/10.1016/j.resconrec.2021.105524.
[3] Z. Zhang, L. Zhang, Y. Yin, X. Liang, A. Li, The recycling of incinerated sewage sludge ash as a raw material for CaO-Al2O3-SiO2-P2O5 glass-ceramic production, Environmental Technology (United Kingdom) 36 (2015) 1098–1103, https://doi.org/10.1080/09593330.2014.982208.
[4] W. Yang, Z. Xu, Y. Wang, Z. Liang, Q. Zhao, Research on combustion characteristics and ash properties of municipal sewage sludge, International Journal of Smart Grid and Clean Energy 8 (2019) 408–414, https://doi.org/10.12720/sgce.8.4.408-414.
[5] M. Kasina, K. Jarosz, M. Stolarczyk, J. Göttlicher, R. Steininger, M. Michalik, Characteristic of phosphorus rich compounds in the incinerated sewage sludge ashes: a case for sustainable waste management, Sci. Rep. 13 (2023), https://doi.org/10.1038/s41598-023-36407-7.
[6] J. Latosińska, Zeolitization of sewage sludge ash with a fusion method, Journal of Ecological Engineering 17 (2016) 138–146, https://doi.org/10.12911/22998993/65463.
[7] H. Herzel, Z. Aydin, C. Adam, Crystalline phase analysis and phosphorus availability after thermochemical treatment of sewage sludge ash with sodium and potassium sulfates for fertilizer production, J Mater Cycles Waste Manag 23 (2021) 2242–2254, https://doi.org/10.1007/s10163-021-01288-3.
[8] A. Assi, F. Bilo, S. Federici, A. Zacco, L.E. Depero, E. Bontempi, Bottom ash derived from municipal solid waste and sewage sludge co-incineration: first results about characterization and reuse, Waste Manag. 116 (2020) 147–156, https://doi.org/10.1016/j.wasman.2020.07.031.
[9] G. Boniardi, A. Turolla, L. Fiameni, E. Gelmi, F. Malpei, E. Bontempi, R. Canziani, Assessment of a simple and replicable procedure for selective phosphorus recovery from sewage sludge ashes by wet chemical extraction and precipitation, Chemosphere 285 (2021), https://doi.org/10.1016/j.chemosphere.2021.131476.
[10] J. Stemann, B. Peplinski, C. Adam, Thermochemical treatment of sewage sludge ash with sodium salt additives for phosphorus fertilizer production - analysis of underlying chemical reactions, Waste Manag. 45 (2015) 385–390, https://doi.org/10.1016/j.wasman.2015.07.029.
[11] Z. Chen, C.S. Poon, Comparative studies on the effects of sewage sludge ash and fly ash on cement hydration and properties of cement mortars, Construct. Build Mater. 154 (2017) 791–803, https://doi.org/10.1016/j.conbuildmat.2017.08.003.
[12] L. Fiameni, A. Fahimi, S. Federici, A. Cornelio, L.E. Depero, E. Bontempi, A new breakthrough in the P recovery from sewage sludge ash by thermochemical processes, Green Chem. 24 (2022) 6836–6839, https://doi.org/10.1039/d2gc02328h.
[13] M. Sall, A. Traoré, A. Ciss Wade, P. Momar Gueye, S. Diouf, G. Dieye, D. Diop, Potential use of sewage sludge ash in lime-based materials, Adv. Mater. 10 (2021) 12, https://doi.org/10.11648/j.am.20211002.11.
[14] L. Świerczek, B.M. Cieślik, P. Konieczka, Challenges and opportunities related to the use of sewage sludge ash in cement-based building materials – a review, J. Clean. Prod. 287 (2021), https://doi.org/10.1016/j.jclepro.2020.125054.
[15] F. Baeza-Brotons, P. Garcés, J. Payá, J.M. Saval, Portland cement systems with addition of sewage sludge ash. Application in concretes for the manufacture of blocks, J. Clean. Prod. 82 (2014) 112–124, https://doi.org/10.1016/j.jclepro.2014.06.072.

[16] G. Rutkowska, P. Wichowski, J. Fronczyk, M. Franus, M. Chalecki, Use of fly ashes from municipal sewage sludge combustion in production of ash concretes, Construct. Build Mater. 188 (2018) 874–883, https://doi.org/10.1016/j.conbuildmat.2018.08.167.
[17] J. Latosińska, Influence of temperature and time of sewage sludge incineration on the mobility of heavy metals, Environ. Prot. Eng. 43 (2017) 105–122, https://doi.org/10.37190/epe170409.
[18] A. Bubalo, D. Vouk, L. Ćurković, M. Rogošić, D. Nakić, C. Cheeseman, Influence of combustion temperature on the performance of sewage sludge ash as a supplementary material in manufacturing bricks, Construct. Build Mater. 404 (2023), https://doi.org/10.1016/j.conbuildmat.2023.133126.
[19] M. Mejdi, M. Saillio, T. Chaussadent, L. Divet, A. Tagnit-Hamou, Hydration mechanisms of sewage sludge ashes used as cement replacement, Cem. Concr. Res. 135 (2020), https://doi.org/10.1016/j.cemconres.2020.106115.
[20] G.P. Sorrentino, R. Guimaraes, A. Cornelio, A. Zanoletti, B. Valentim, E. Bontempi, Mitigating CO2 emissions through an industrial symbiosis approach: leveraging cork ash carbonation, Heliyon 10 (2024), https://doi.org/10.1016/j.heliyon.2024.e32893.
[21] G. Biava, L.E. Depero, E. Bontempi, Accelerated carbonation of steel slag and their valorisation in cement products: a review, Spanish Journal of Soil Science 14 (2024), https://doi.org/10.3389/sjss.2024.12908.
[22] K. Kim, D. Kim, Y. Na, Y. Song, J. Wang, A review of carbon mineralization mechanism during geological CO2 storage, Heliyon 9 (2023), https://doi.org/10.1016/j.heliyon.2023.e23135.
[23] X. Liu, X. Liu, Z. Zhang, X. Ai, Effect of carbonation curing on the characterization and properties of steel slag-based cementitious materials, Cem. Concr. Compos. 154 (2024), https://doi.org/10.1016/j.cemconcomp.2024.105769.
[24] S.Y. Pan, Y.H. Chen, L.S. Fan, H. Kim, X. Gao, T.C. Ling, P.C. Chiang, S.L. Pei, G. Gu, CO2 mineralization and utilization by alkaline solid wastes for potential carbon reduction, Nat Sustain 3 (2020) 399–405, https://doi.org/10.1038/s41893-020-0486-9.
[25] DECRETO LEGISLATIVO 3 aprile 2006, n. 152 - Norme in materia ambientale, https://www.gazzettaufficiale.it/atto/stampa/serie_generale/originario, 2006.
[26] G. Montes-Hernandez, R. Pérez-López, F. Renard, J.M. Nieto, L. Charlet, Mineral sequestration of CO2 by aqueous carbonation of coal combustion fly-ash, J. Hazard. Mater. 161 (2009) 1347–1354, https://doi.org/10.1016/j.jhazmat.2008.04.104.
[27] Y. Feng, X. Li, H. Wu, C. Li, M. Zhang, H. Yang, Critical review of Ca(OH)2/CaO thermochemical energy storage materials, Energies (Basel) 16 (2023), https://doi.org/10.3390/en16073019.
[28] A.A. Khosa, C.Y. Zhao, Heat storage and release performance analysis of CaCO3/CaO thermal energy storage system after doping nano silica, Sol. Energy 188 (2019) 619–630, https://doi.org/10.1016/j.solener.2019.06.048.
[29] E. Miao, Y. Du, X. Zheng, X. Zhang, Z. Xiong, Y. Zhao, J. Zhang, Kinetic analysis on CO2 sequestration from flue gas through direct aqueous mineral carbonation of circulating fluidized bed combustion fly ash, Fuel 342 (2023), https://doi.org/10.1016/j.fuel.2023.127851.
[30] G.P. Sorrentino, R. Guimarães, B. Valentim, E. Bontempi, The influence of liquid/solid ratio and pressure on the natural and accelerated carbonation of alkaline wastes, Minerals 13 (2023), https://doi.org/10.3390/min13081060.
[31] Y. Xu, H. Hu, J. Liu, J. Luo, G. Qian, A. Wang, PH dependent phosphorus release from waste activated sludge: contributions of phosphorus speciation, Chem. Eng. J. 267 (2015) 260–265, https://doi.org/10.1016/j.cej.2015.01.037.
[32] L. Luyckx, J. Van Caneghem, Recovery of phosphorus from sewage sludge ash: influence of chemical addition prior to incineration on ash mineralogy and related phosphorus and heavy metal extraction, J. Environ. Chem. Eng. 10 (2022), https://doi.org/10.1016/j.jece.2022.108117.
[33] C.A. Quist-Jensen, L. Wybrandt, H. Løkkegaard, S.B. Antonsen, H.C. Jensen, A. H. Nielsen, M.L. Christensen, Acidification and recovery of phosphorus from digested and non-digested sludge, Water Res. 146 (2018) 307–317, https://doi.org/10.1016/j.watres.2018.09.035.
[34] L. Luyckx, S. Geerts, J. Van Caneghem, Closing the phosphorus cycle: multi-criteria techno-economic optimization of phosphorus extraction from wastewater treatment sludge ash, Sci. Total Environ. 713 (2020), https://doi.org/10.1016/j.scitotenv.2019.135543.
[35] L. Luyckx, D.S. Sousa Correia, J. Van Caneghem, Linking phosphorus extraction from different types of biomass incineration ash to ash mineralogy, ash composition and chemical characteristics of various types of extraction liquids, Waste Biomass Valoriz. 12 (2021) 5235–5248, https://doi.org/10.1007/s12649-021-01368-3.
[36] X. Weichang, L. Xuanyong, Z. Xuebin, D. Chuanxian, Effect of hydroxyapatite coating crystallinity on dissolution and osseointegration in vivo, J. Biomed. Mater. Res. 74A (2005) 553–561.
[37] S. Wu, J. Cao, Q. Shao, How to select remanufacturing mode: end-of-life or used product? Environ. Dev. Sustain. (2024) https://doi.org/10.1007/s10668-024-04515-7.